



# A wireless, skin-integrated system for continuous pressure distribution monitoring to prevent ulcers across various healthcare environments



Seonggwang Yoo<sup>1,2,3,4,20</sup>, Zengyao Lv<sup>5,20</sup>, Nicholas Fadell<sup>6,20</sup>, Jae-Young Yoo<sup>1,7,20</sup>, Seyong Oh<sup>1,8,20</sup>, Kyoung-Ho Ha<sup>1,20</sup>, William M. Moritz<sup>6</sup>, Jihun Cha<sup>9</sup>, Hanbing Wu<sup>1</sup>, Jihun Park<sup>1</sup>, Sung Soo Kwak<sup>10</sup>, Kyeongha Kwon<sup>11</sup>, Yoonseok Park<sup>12</sup>, Donghwi Cho<sup>13,14</sup>, Hak-Young Ahn<sup>1</sup>, Chanho Park<sup>1</sup>, Sangjun Kim<sup>15</sup>, Tae Wan Park<sup>1</sup>, Woo-Youl Maeng<sup>1</sup>, Heung Cho Ko<sup>9</sup>, Amanda M. Westman<sup>6</sup>, Matthew MacEwan<sup>6</sup>, Yonggang Huang<sup>5,16</sup>✉, Justin Saks<sup>6</sup>✉ & John A. Rogers<sup>1,5,16,17,18,19</sup>✉

Pressure ulcers remain a persistent challenge in healthcare, particularly for individuals with limited mobility or compromised sensation. Early detection is critical to prevent ischemic damage leading to necrosis, infections, and prolonged hospital stays. Conventional sensing technologies that integrate into the mattress, while effective in gathering data on pressure distributions, are restricted to stationary environments, and they can miss significant periods when patients leave their beds or shift positions. Furthermore, these systems do not offer consistent information on the specific spatial distribution of pressure across the body, because the sensors integrate with the mattress and not the body. Recent research establishes capabilities in soft, skin-interfaced wireless alternatives, but in designs that require specialized processes and materials that might not scale effectively for practical production and use. Here, we present a wireless, skin-integrated pressure monitoring system that mounts on the skin, in anatomically matched forms and with soft mechanical interfaces, for continuous data collection. This platform, built on manufacturable components and designs, features an array of soft, elastomer-encapsulated pressure sensors that minimize discomfort, with wireless communications and an independent power management system to enable operation across diverse healthcare settings, including homes, outpatient facilities, and operating rooms, all without physical tethers. Additionally, an external alarm satellite device delivers vibratory and visual alerts if predefined pressure thresholds are exceeded, guiding caregivers or patients to take timely action. Experimental and finite element analysis support the design principles, and deployments on patients in hospital settings illustrate modes for practical use.

Pressure ulcers occur when prolonged sources of pressure hinder blood flow to the skin and underlying tissues, resulting in ischemia and tissue necrosis<sup>1,2</sup>. Individuals at high risk include those confined to a bed, wheelchair users, or those with reduced sensation or poor nutrition. Bony areas such as the sacrum, heels, elbows, and hips are particularly vulnerable to pressure ulcer development due to the compression of soft tissues between skeletal structures and external surfaces<sup>2</sup>. Although standard care protocols

—including regular repositioning<sup>3</sup>, specialized mattresses<sup>4,5</sup>, and manual assessments (e.g., Braden Scale)<sup>6</sup>—aim to mitigate these risks, pressure ulcers remain a significant clinical and economic concern. In their early stages, these ulcers may manifest only as persistent redness or minor abrasions, which can be easily overlooked or misdiagnosed. Progression often leads to deep tissue injury and infection. In severe cases, life-threatening complications like sepsis can occur<sup>7-9</sup>. The reliance on visual

A full list of affiliations appears at the end of the paper. ✉e-mail: [y-huang@northwestern.edu](mailto:y-huang@northwestern.edu); [jmsacks@wustl.edu](mailto:jmsacks@wustl.edu); [jrogers@northwestern.edu](mailto:jrogers@northwestern.edu)

inspections and subjective assessments highlights the necessity for quantitative, continuous methods to monitor early tissue degradation and changes in mechanical stress.

Most previous research on monitoring and preventing pressure ulcers involves specialized support surfaces, such as mattress-based systems with integrated arrays of pressure sensors to collect data on pressure distributions<sup>10,11</sup>. Although these systems demonstrate that quantitative monitoring can significantly reduce ulcer formation by prompting caregivers to reposition patients, they remain limited by their static nature; patients frequently leave the bed or change positions, resulting in unmonitored intervals and an inability to accurately track specific body locations.

To address these limitations, more recent efforts focus on wearable, skin-integrated pressure monitoring technologies<sup>12–16</sup>. Several rely, however, on near-field communication-based schemes and wireless power transfer strategies, both of which require close-range interaction with external wireless equipment. In contrast, the present platform incorporates Bluetooth Low Energy (BLE), which supports autonomous, long-range operation (~10 m) with smartphones, eliminating the need for external coils or bedside systems. In addition, most of these and related approaches involve individual sensors, deployed separately at multiple locations of concern, using designs and materials that are applicable for research purposes but might not align effectively with scaled manufacturing approaches. Both such schemes offer important capabilities, but also have some shortcomings for practical use.

The present work introduces three key advances to allow practical clinical deployment: (i) a BLE communication platform that supports autonomous, long-range operation with standard smartphones, eliminating the need for specialized bedside hardware, (ii) a scalable architecture that integrates an array of sensors into a single device to provide high-resolution spatial pressure mapping, and (iii) a skin-safe, patient-compatible form factor with a built-in visual and vibratory alerts to prompt timely posture adjustments. These features move beyond previous proof-of-concept demonstrations to yield a wireless, skin-integrated solution suitable for real-world ulcer prevention and long-term monitoring.

This skin-integrated pressure monitoring and spatial mapping system that operates wirelessly and autonomously using standard Bluetooth technology in nearly any environment—home, hospital, or outdoors. By circumventing reliance on specialized hospital beds or wheelchairs, this approach extends continuous pressure monitoring beyond traditional settings. The wireless architecture eliminates cumbersome tethers, enabling real-time data transmission to a mobile device user interface. Moreover, rather than depending on a single or minimal set of separate sensors, the system employs an array of pressure sensors to capture a distribution map of the targeted region<sup>15</sup>. This spatial detail facilitates comprehensive data analysis, allowing clinicians and caregivers to detect posture shifts, address asymmetric loading due to skeletal misalignment, and identify subtle pressure hotspots that might go unnoticed. By pinpointing these pressure distributions in real-time, the system offers an important tool for proactive care and timely intervention, potentially reducing the generation of pressure ulcers and thus improving patient outcomes. The designs and components are selected specifically for their practical use and potential for scaled production.

As an additional feature that further enhances patient safety, an external alarm satellite unit provides visual and vibratory alerts upon detection of pressure values and time intervals that exceed predefined thresholds, set by the physician to capture magnitudes and temporal durations that represent significant risk. Finite element analysis (FEA) confirms the compatibility of this system with the skin and surrounding tissues. Designs guided by this modeling ensure consistent performance under repeated mechanical loading, temperature fluctuations, and prolonged use, as demonstrated experimentally. By integrating comfortably with the body and providing automated feedback, this system shows promise as a means to reduce pressure ulcer prevalence and improve patient care across a wide range of healthcare settings.

## Results

### Wireless, skin-integrated pressure monitoring system

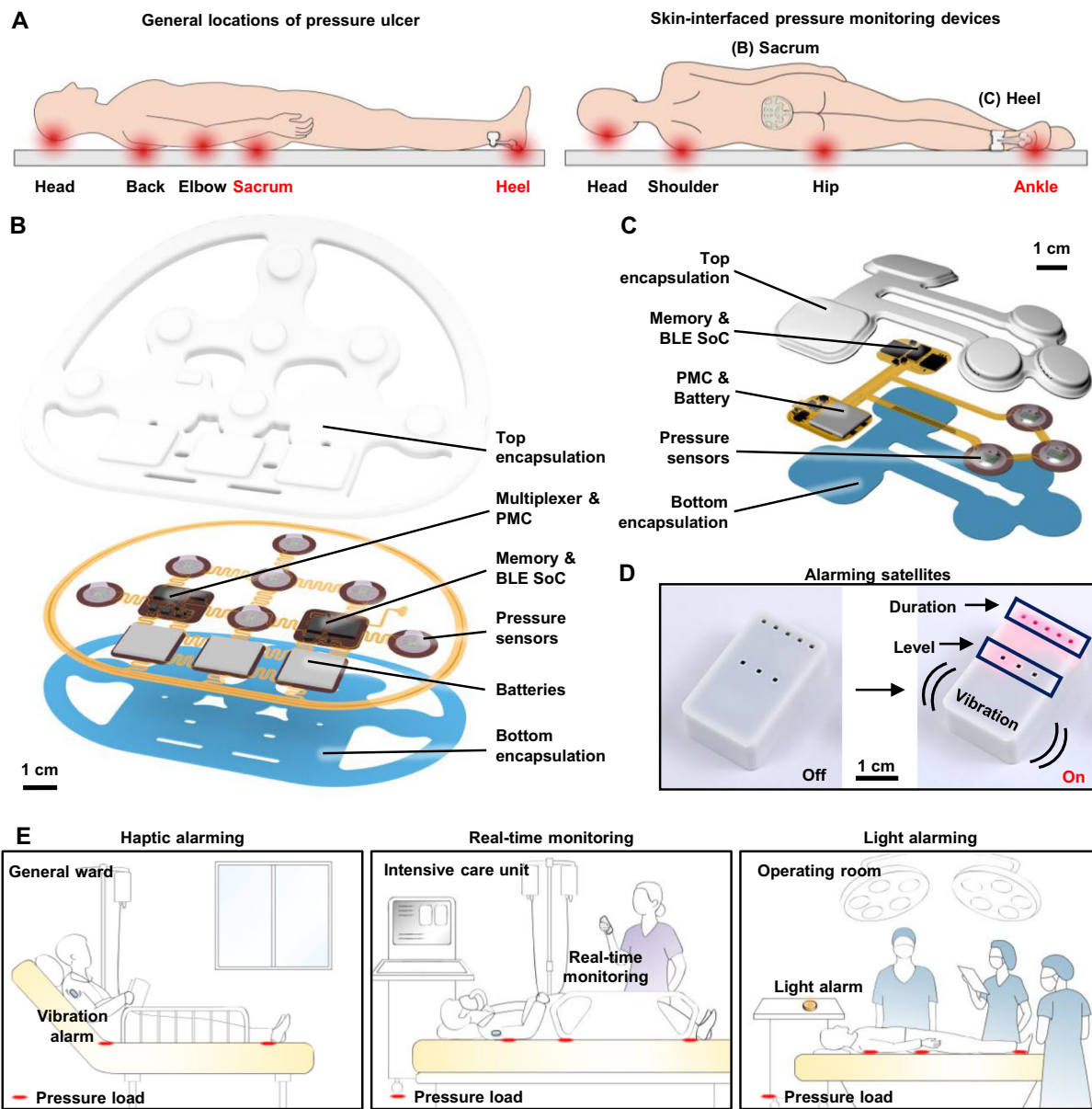
The pressure monitoring system consists of three main components: (1) a skin-integrated pressure monitoring device, (2) a mobile device with a user interface for system control and communication, and (3) a satellite wirelessly connected unit that alerts patients or caregivers when pressure levels and time intervals exceed a predefined threshold. Figure 1A illustrates the areas most susceptible to pressure ulcers, particularly the sacrum and heel, where skin-integrated pressure monitoring devices with anatomically matched layouts can be positioned to alert caregivers to the potential for ulcer formation. These high-risk areas also include the head, back, elbows, and ankles, where related types of monitoring systems could be effectively used. The design conforms to the contours of each region, featuring multiple pressure sensors strategically placed in arrays across the most vulnerable locations.

Figure 1B, C shows schematic, exploded view illustrations of devices designed for the sacrum and heel, respectively. The pressure sensors rely on modifications to commercial system-on-chip (SoC) barometers (TE Connectivity, MS5611)<sup>17,18</sup>. Here, removal of the metal cap exposes the piezo-resistive strain gauge membrane to allow introduction of a liquid prepolymer to an elastomer. Curing forms a soft, solid structure that can transfer mechanical pressure imposed from the surroundings onto the membrane. Careful designs ensure that the range over which pressures can be measured accurately with such devices aligns with clinical requirements. Each sensor module created in this manner measures both pressure and temperature at its respective location. A BLE SoC (Insight SIP, ISP1807) manages the operation of the system using a multiplexer to control seven sensors and to wirelessly transfer data to a mobile device. A memory chip (Micron Technology Inc., MT29F2G01) records the pressure and temperature data, which are also wirelessly transmitted via the BLE SoC to a mobile device, enabling both onboard storage and real-time communications. Three small, rechargeable lithium polymer batteries (DNK Power, DNK201515, 20 mAh) supply power. A radio frequency coil and battery charging circuit (Texas Instruments, BQ25101) enable wireless recharging. During continuous operation with data transmission every 1 s, the device consumes ~150 µA, supporting over 2 weeks (~16 days) of monitoring. Extending the transmission interval to 30 s significantly reduces the average current consumption to ~21 µA, resulting in an operational lifetime of ~115 days. Further reductions in power consumption are achievable when the device operates using memory only, where the data are saved internally without wireless transmission. (Fig. S1). All components, including the pressure sensor, BLE SoC, memory, battery, and power management circuitry on the fabricated printed circuit board (FPCB), are mounted within an elastomeric enclosure formed by top and bottom layers of silicone (Silbione RTV 4420) to ensure safety in clinical environments. The internal cavity formed by the bonding of these layers is filled with an uncured polyorganosiloxane elastomer (Ecoflex 00-30), cured at room temperature for 24 h. Additional details on device fabrication are in the “Methods” section.

Figure 1D shows the satellite unit mentioned previously, which features a vibrating actuator and light-emitting diodes for haptic and visual alerts, respectively. These alerts activate at magnitudes and frequencies that correspond to user-defined levels of risk inferred from the time-dependent measurements of pressure. The system supports various hospital environments, including haptic alerts for patients in general wards, real-time monitoring in intensive care units, and visual alerts during surgeries (Fig. 1E). Caregivers or users can customize alert thresholds based on the conditions of the patient. This flexibility allows the device to alert for potential pressure ulcer formation across multiple care settings by providing continuous monitoring and timely feedback.

### Soft pressure sensor for body pressure monitoring

Robust and reliable operation is essential, without drift or damage across repeated loading and unloading cycles, throughout long-term, high-load conditions, and during temperature fluctuations<sup>19–21</sup>. As mentioned previously, the sensors introduced here rely on custom modifications of



**Fig. 1 | Wireless, skin-integrated pressure monitoring system to help prevent pressure ulcers.** A Schematic illustrations of general locations of pressure ulcer generation and the skin-integrated pressure monitoring devices on the sacrum and heel. B, C Schematic illustrations of an exploded view of skin-integrated pressure monitoring devices for sacrum and heel. D A satellite unit provides alerts of the risk of pressure ulcers by vibration and light emission. E Use scenarios of a pressure monitoring and alerting system to prevent ulcer generation in various hospital settings.

monitoring devices for sacrum and heel. D A satellite unit provides alerts of the risk of pressure ulcers by vibration and light emission. E Use scenarios of a pressure monitoring and alerting system to prevent ulcer generation in various hospital settings.

commercial barometric pressure sensors (Fig. 2A). The specific design uses a truncated cone-shaped silicone elastomer molded above, as described in the “Methods” and Fig. S2. FEA simulations demonstrate that pressure applied through elastomer compression induces mechanical strains that correspondingly change the resistance of the piezoresistive microelectromechanical membrane structure, enabling accurate pressure sensing (Fig. 2B). These simulations validate mechanisms for the translation of mechanical deformations into electrical signals by resistance changes. Moreover, the uniform pressure distribution across the sensor membrane guarantees consistent and accurate readings, with pressure distributions between 8.7 and 11 kPa when applied at 10 kPa (Fig. 2C). To mitigate potential signal drift caused by fluctuations in body temperature, the SoC utilizes an integrated temperature sensor and temperature compensation algorithm to maintain stable and accurate pressure measurements. Recalibration after encapsulation involves revision of the constants in the compensation algorithm to reflect the effects of removal of the metal cap, application of a silicone elastomer layer, and complete

encapsulation in the final device. In addition, a calibration process for each sensor in the array allows those with parameters that lie outside the target sensitivity range to be replaced, resulting in a final array with uniform performance. The supporting data in Fig. S3 present calibration curves of the seven sensors and confirm minimal inter-sensor variability, underscoring the reproducibility and robustness of the platform. Accurate and long-term pressure monitoring remains a persistent challenge for traditional thin-film pressure sensors due to their susceptibility to mechanical deformation and thermal drift. The engineered barometric sensor introduced here overcomes these limitations through robust structural design and integrated compensation features, as demonstrated in the following set of experimental results. The data in Fig. 2D show a linear correlation between the loading and unloading cycles, with no measurable hysteresis. The design of the elastomer structure allows for modulation of the sensitivity and sensing range of the sensor. In this study, an elastomer structure with a height of 2 mm, a 5 mm diameter at the top, and 10 mm at the base provides a sensing range of 0–40 kPa, which covers the range of

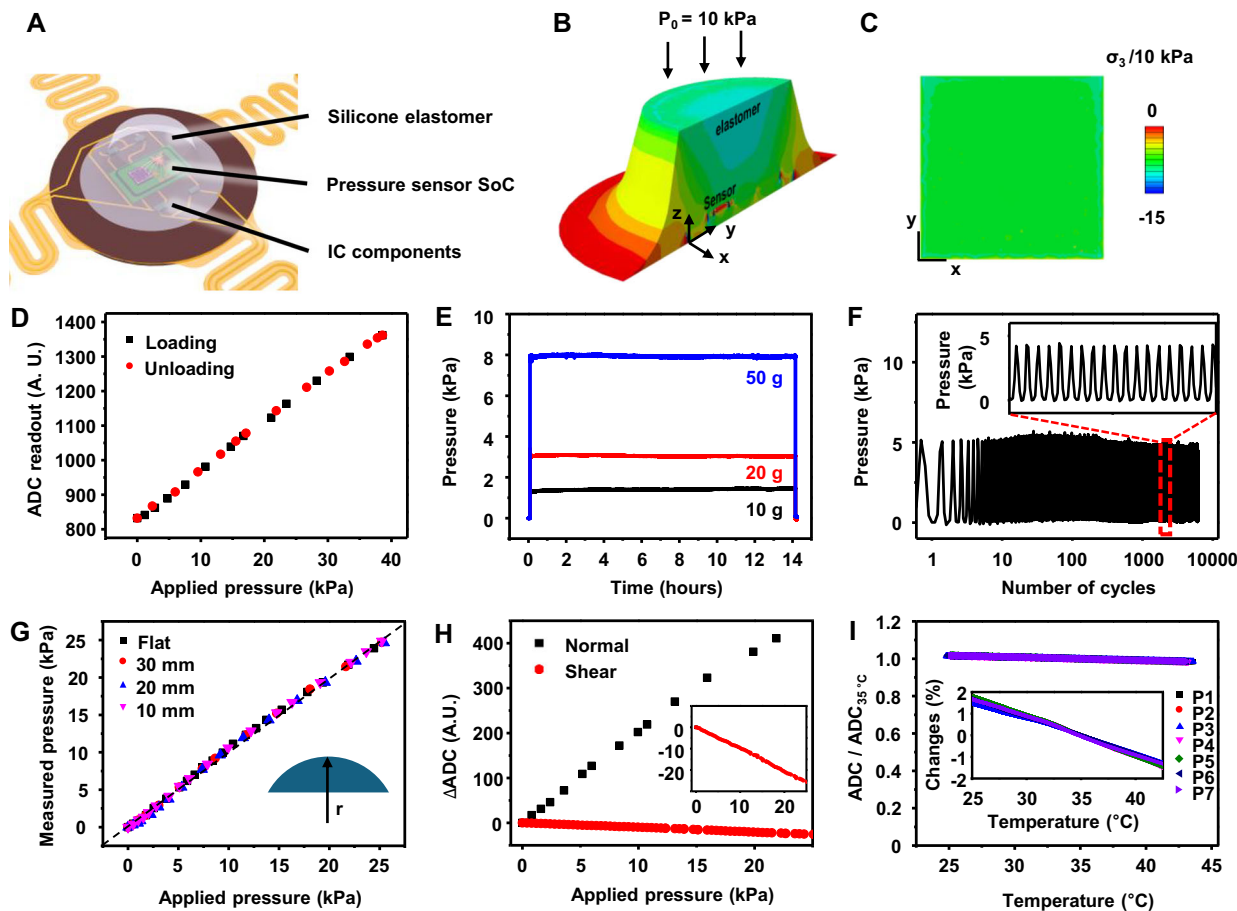


**Fig. 2 | Performance and characterization of a soft, elastomer-encapsulated pressure sensor.** **A** Illustration of the design features of the soft elastomer-encapsulated pressure sensor, showing the internal components, including the pressure sensing element, encapsulating elastomer, and connection circuitry. **B, C** Finite element analysis (FEA) simulation of the stress distribution of the pressure sensor. **B** shows the stress distribution within the elastomer structure, and **C** provides a stress distribution of the surface of the sensor membrane under pressure. **D** Linear response of the sensor during loading and unloading cycles with

minimal hysteresis. **E** Long-term stability of the pressure sensor under continuous loads of 10, 20, and 50 g, corresponding to pressure values of 1.54, 3.08, and 7.70 kPa, respectively. **F** Pressure response of the sensor after approximately 5000 cycles of loading and unloading. **G** Sensor performance on curved substrates shows that the pressure response remains consistent when compared to measurements on flat substrates. **H** Shear stress stability of the sensor compared to the normal stress. **I** Temperature response of seven pressure sensors in the device.

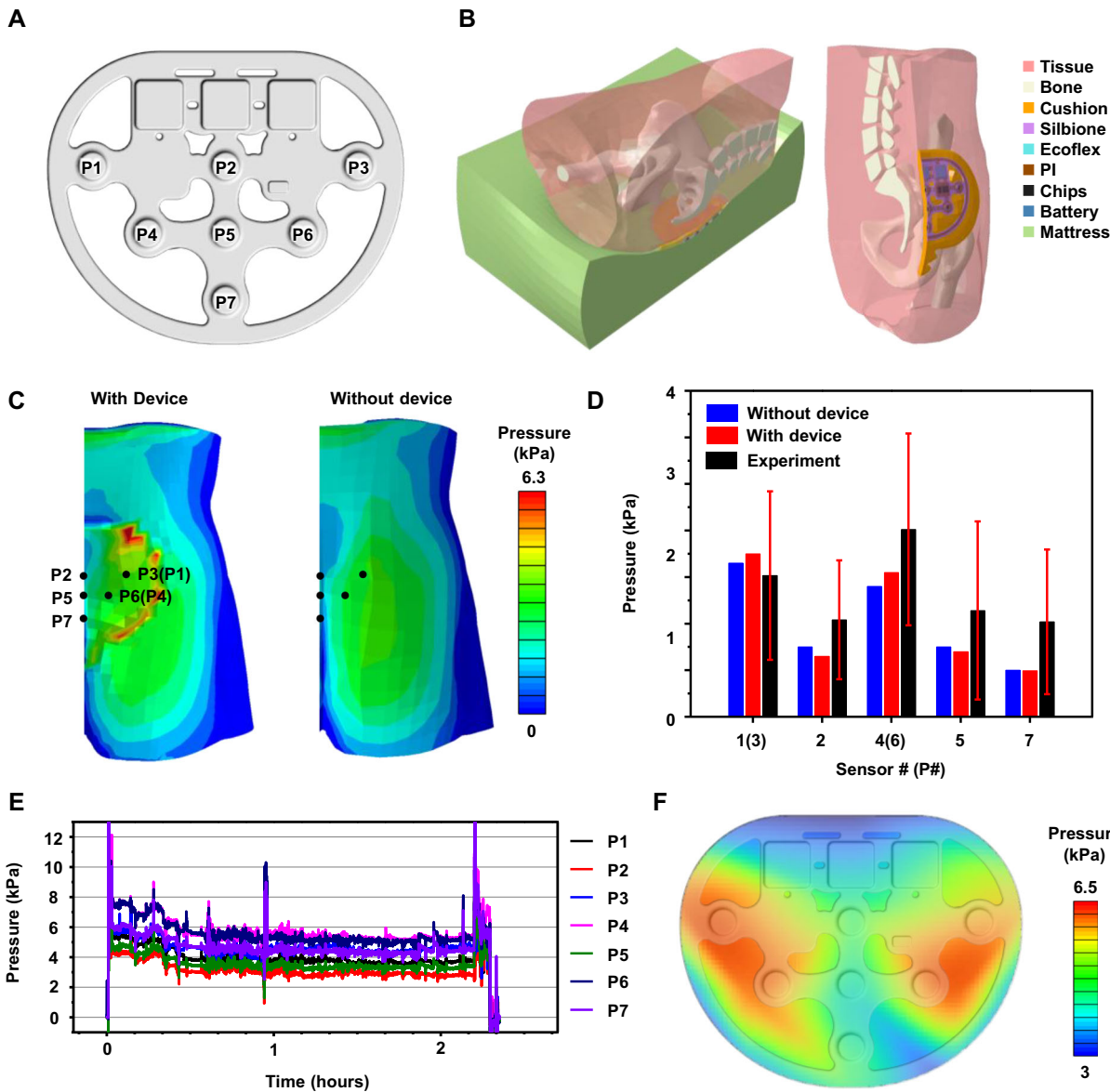
body pressures of relevance here. Figure 2E shows the long-term stability of the pressure sensor, with constant pressure loads of 10, 20, and 50 g by weight, corresponding to pressure values of 1.54, 3.08, and 7.70 kPa, respectively. The results show a minimal drift rate, with an output that remains within  $\pm 2\%$  of the initial value after 12 h of continuous monitoring. This stability is crucial for applications that require prolonged pressure monitoring, such as during sleep or in clinical environments where consistent pressure readings are necessary to prevent pressure ulcers. Regarding durability, Fig. 2F shows that the sensor exhibits minimal variation in its response after 5000 cycles of loading and unloading at a pressure of 5 kPa. The elastomer allows the sensor to recover its original shape and to resist permanent deformation, even after extended periods under load. As a result, the sensor maintains accurate and consistent pressure measurements over time without the need for recalibration. Regarding flexibility, the performance is unchanged for bending to a radius of down to 10 mm, which covers the typical human body curvatures (Fig. 2G). The results in Fig. 2H show the response to the shear forces with a 5% variation compared to normal stress conditions. This minimal change indicates that the sensor can maintain reliable performance even when exposed to complex loading conditions, including shear stress. The ability to resist performance degradation under shear forces is critical for ensuring accurate pressure monitoring in dynamic environments, such as during movement or repositioning. As shown in

Fig. 2I, the sensor maintains consistent pressure readings across the temperature range of human skin (within 2% from 25 to 45 °C).

#### Skin-integrated pressure monitoring system

Figure 3A shows a photograph of a sacral pressure monitoring device with labels of pressure sensor sites (P1–P7). The device is directly interfaced with the skin of a patient lying on a hospital bed. The device incorporates a soft cushion that protects the skin and reduces the risk of pressure injuries<sup>22,23</sup>, particularly in the sacral region, which is highly vulnerable to pressure accumulation. Additional FEA-based compressive analysis (Fig. S4A) characterizes the system performance with the integrated cushion. The results (Fig. S4B, C) quantify the uniformity of the force distribution of the complete device-cushion assembly. Bending and twisting tests confirm that the device adheres to the cushion without introducing high strain (Fig. S4D–I). The inset image highlights the strategic placement of seven sensors (P1–P7) across key anatomical locations: P1 (Upper left), P2 (Upper center), P3 (Upper right), P4 (Middle left), P5 (Middle center), P6 (Middle right), and P7 (Bottom). Each sensor targets a region prone to pressure buildup, enabling real-time assessment of pressure injury risk.

Figure 3B presents an FEA model to evaluate the mechanical interaction between the pressure monitoring device and the skin. The simulation includes layers representing human tissue, bone, the soft cushion, the mattress, and the structural components of the device, including silbione, ecoflex,



**Fig. 3 | Pressure distribution on the skin interface at the sacrum.** A Photograph of a sacral pressure monitoring device with labels of pressure sensor sites (P1–P7).

**B** FEA simulation models for pressure distributions at the skin interface for a subject lying on a bed. **C** Pressure distribution at the sacrum with and without the device.

**D** Comparison of pressure at each sensor location with and without the device.

**E** Representative pressure profiles of a patient lying on a bed in the operating room. **F** Areal mapping of the average pressure measurement from (E). The cushion is made of soft polymer foam, and its elastic modulus is given in Table S3.

polyimide, components, and batteries. The FEA results and experimental measurements, as shown in Fig. 3C, D, involve realistic loading conditions, with the subject lying supine on a standard hospital mattress. Figure 3C, D show that pressure loads at the sensor sites (P1–P7) remain largely consistent, comparable to those measured without the device. The device architecture features a punctured, stretchable design that enhances breathability and minimizes localized stress. The localized increase observed in Fig. 3C originates primarily from the adhesive layer of the cushion pad rather than the device itself. For example, pressure at P1 and P3 are 3.3 kPa without the device and 3.5 kPa with it; P2 shows 1.5 and 1.3 kPa, respectively; P4 and P6 increase slightly from 2.8 to 3.1 kPa; P5 shows a minor decrease from 1.5 to 1.4 kPa; and P7 remains nearly unchanged (1.0 vs. 0.99 kPa). Notably, sensors P1 and P4 display relatively higher pressure values, consistent with their load-bearing anatomical locations. Simulation values align well with experimental data (averaged values from 7 clinical trials, Tables S1 and S2), with deviations at P1 (+17%), P4 (−23%), P2 (−38%), P5 (−39%), and P7 (−51%), all within acceptable experimental variance ( $\pm\sigma$ ). The cushion does

not require customization for individual anatomies, as the pressure change induced by its presence is minimal (Fig. 3D).

Other versions of this device architecture enable localized pressure monitoring in anatomically complex regions, such as the heel (Fig. S5A, B). Replacing Silbione (modulus  $E$ : 800 kPa) with Ecoflex (modulus  $E$ : 60 kPa) for the encapsulation layer softens the device, resulting in a 3% decrease in maximum skin pressure from 7.3 to 7.1 kPa (Fig. S5C). Adjusting the cushion geometry to align the outer surface of the device with the cushion plane eliminates protrusions and further reduces peak pressure by 4% (from 7.1 to 6.8 kPa). In addition, by selectively adjusting the modulus of the cushion, particularly in the regions that directly interface with the device (Fig. S5D) to closely match that of human tissue (Fig. S5E), the system achieves a minimum pressure of 5.4 kPa, representing a 21% reduction (Fig. S5F). The modulus of the cushion depends on the relative density (or porosity) of the foam<sup>24–28</sup>, commonly controlled via variation of the chemical blowing agent content during foam fabrication<sup>29</sup> to attain mechanical properties approximating those of human soft tissue.

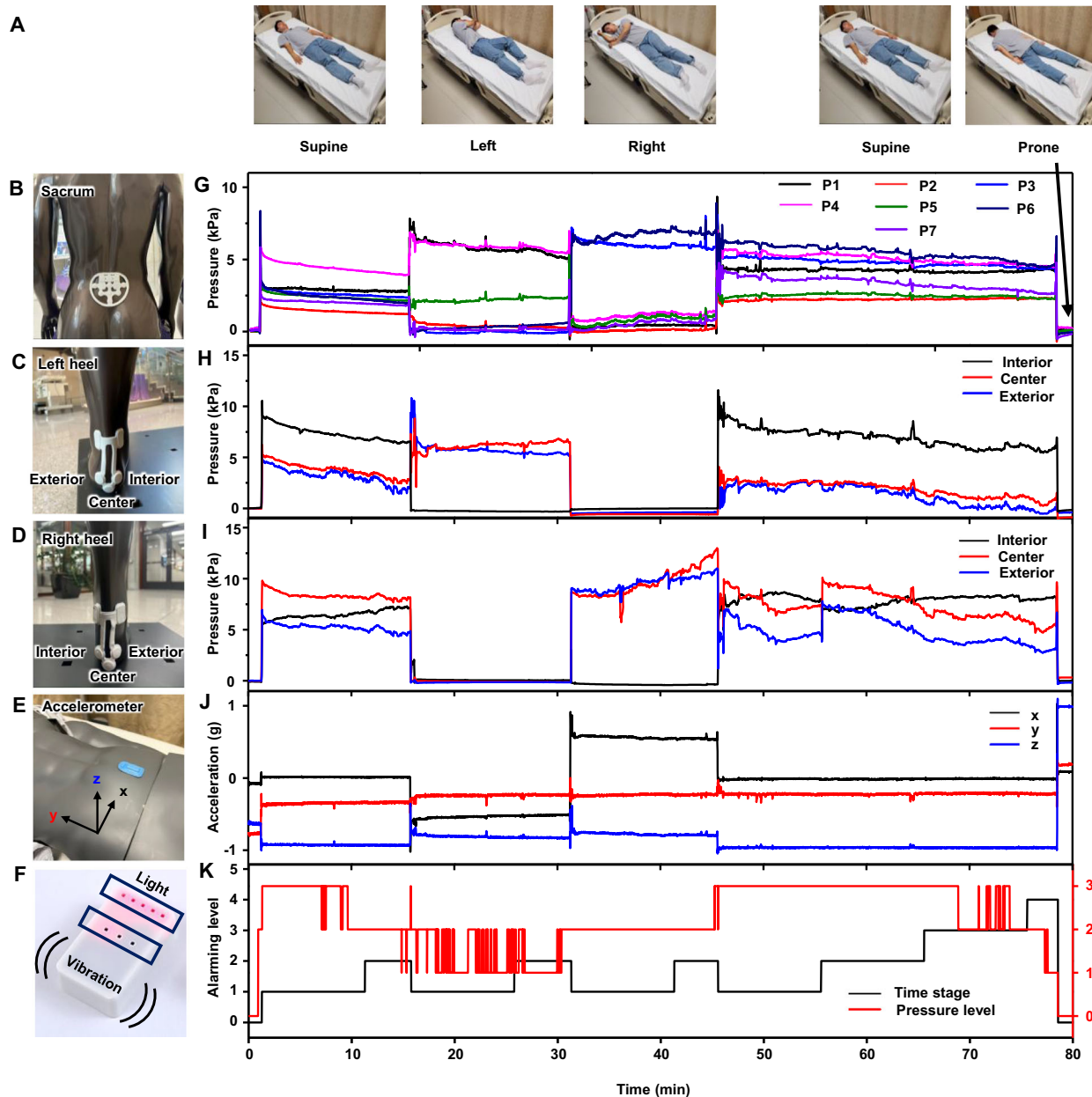


**Fig. 4 | Pressure monitoring and alarming feedback for posture change.**

A Photographs of a subject in different postures. B–D Photographs of the devices at each location and G–I the continuous monitoring of B sacrum, C left heel, and D right heel pressure. E Photographs of an accelerometer attached to the lower

stomach, and J the acceleration data associated with posture changes of the subject. F Photograph of a satellite unit designed to alert the average pressure level and the time duration without posture changes, as well as K alarm level (Time stage, and Pressure level) associated with the pressure monitoring.

The final optimized configuration combines materials and geometric refinements to achieve a 28–40% pressure reduction compared to the initial design. As shown in Fig. S5G, pressure readings at sensor sites in the optimized configuration closely matched those of the cushion alone, differing by only 1–5%. These modular and adaptive design strategies offer broad applicability across anatomical sites beyond the heel for patient-specific pressure monitoring needs.

Figure 3E displays real-time pressure monitoring profiles collected in a hospital environment. The data correspond to continuous recordings for over two hours across all sensor locations (P1–P7), with the patient in a supine state. Dynamic pressure variations reflect subtle postural shifts, small movements, and redistribution of body weight<sup>30</sup>. At approximately 1 h, transient fluctuations appear due to larger body movements, as confirmed in the expanded profile (54–59 min) in Fig. S6. Higher values occur at P1, P3, P4, and P6, corresponding to regions near the buttocks

that bear most body weight. In contrast, P2, P5, and P7 display relatively lower pressures, indicating areas with less direct load or those supported by the structural design of the cushion. This continuous monitoring capability provides critical data for identifying time-dependent pressure changes and detecting potential high-risk zones for pressure ulcer development, enabling timely clinical intervention. Figure 3F represents a visualized average pressure distribution derived from the time-series data in Fig. 3E. The pressure map uses a gradient color scale, where red indicates areas of higher pressure and blue represents lower pressure. The results demonstrate that soft tissue regions, such as the buttocks, experience concentrated pressure, consistent with the weight-bearing nature of these areas. In contrast, regions over bony prominences or areas with thin soft tissue exhibit reduced pressure values. This mapping provides an intuitive spatial overview of the pressure distribution, facilitating the identification of high-risk regions prone to pressure ulcers. The observed

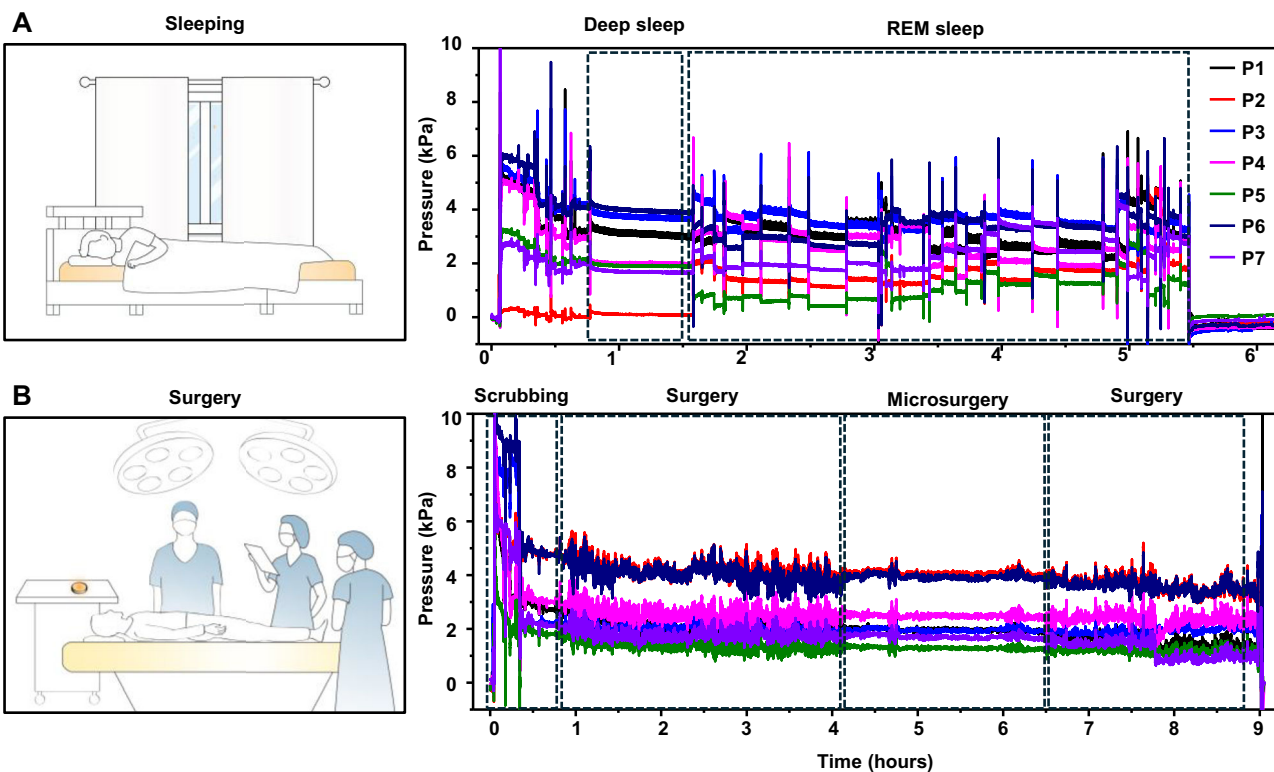


**Fig. 5 | Pressure monitoring on the sacrum in various scenarios. A** Pressure monitoring during sleep. **B** Pressure monitoring during plastic surgery.

trends align well with the simulation results, reinforcing the ability of the device to accurately capture pressure profiles in clinical settings.

#### Continuous pressure monitoring and alarming feedback system

Figure 4 focuses on the continuous pressure monitoring system and its alarm feedback mechanism. Posture changes, such as from supine to left or right lying positions, lead to redistributions of pressure. Continuous monitoring at multiple locations provides valuable data for evaluating health risks and detecting areas vulnerable to pressure injuries. Figure 4A illustrates posture changes between supine, left-side, and right-side lying positions. The system integrates multi-channel pressure monitoring devices to cover the sacrum (Fig. 4B) and both heels (Fig. 4C, D). The sacrum device incorporates seven sensors (P1–P7), while each heel device features three sensor channels (Interior, center, and exterior). These devices are independently capable of detecting pressure levels, posture, and weight distribution, ensuring precise and localized monitoring of pressure dynamics. Figure 4G–I presents the continuous recordings of pressure values collected at each sensor location, sampled at a rate of 1 Hz. The data reveal distinct patterns of pressure distribution depending on posture change. When lying supine, the pressure distributes evenly across the sacrum and heels. In the left or right side-lying positions, however, the pressure becomes asymmetrically distributed, concentrating on the side in contact with the bed. The sacrum and heel sensors capture this biased distribution to provide quantitative insights into how posture affects pressure levels in different regions (Fig. S7).

Figure 4J presents data obtained from an accelerometer shown in Fig. 4E, strategically placed on the lower abdomen. This device monitors postural changes in real-time by capturing accelerations along the *x*, *y*, and *z* axes relative to the gravitational vector. The results provide a comprehensive analysis of both pressure dynamics and postural shifts, with associated alerts that pass through the satellite unit (Fig. 4F). As shown in Fig. 4K, increasing exposure to pressure causes heightened light and vibration alert levels, thereby prompting individuals, on their own or with the assistance of healthcare providers, to adjust their posture to reduce the risk of pressure injuries. This

demonstration involves two alarm logics: (i) a pressure-based alert, increasing by one step for every 2 kPa rise in averaged pressure, and (ii) a time-based alert, increasing by one step for every 10 min without posture change. These values serve as illustrative examples, rather than standardized clinical thresholds, and can be adjusted according to patient-specific or guideline-based needs.

#### Pressure monitoring in various scenarios

Practical demonstrations systematically monitor pressure across diverse environments. The soft and wireless configurations of these devices enable subjects to wear them comfortably in settings from an operating room to a bed at home during sleep. Figure 5A illustrates pressure monitoring in this latter case, for a healthy adult volunteer. The system captures time-series pressure data, correlating with sleep stages identified through a smartwatch. During deep sleep, the pressure data displays stable and consistent patterns of minimal movement. Conversely, during REM sleep, the pressure signals exhibit significant fluctuations, reflecting frequent changes in posture<sup>31,32</sup>. Figure 5B presents pressure data from a patient undergoing surgery, showing distinct pressure dynamics during different procedure phases, including scrubbing, operating, and microsurgery. The time-series data delineate distinct characteristics for each phase, reflecting pressure dynamics and patient positioning during extended procedures. Unlike conventional mattress-based pressure monitoring systems that require placement on the surgical bed—an approach often limited by sterility, restricted space, and workflow constraints—the wearable platform introduced here eliminates the need for bulky external installations and operates autonomously via BLE. The technology is thus practical for continuous monitoring during surgery as well as in daily settings such as home beds or chairs. Such data are essential for identifying high-risk areas where prolonged pressure could result in tissue damage<sup>23</sup>. In both scenarios, retrospective analysis of historical pressure profiles supports investigation into the relationship between ulcer development and sustained localized pressure, thereby advancing evidence-based prevention strategies. These capabilities highlight the contribution of the system beyond immediate repositioning, delivering both real-time alerts and actionable longitudinal

data critical for reducing pressure-related tissue injury in environments where patient movement is restricted.

## Discussion

This paper presents a soft, wireless, skin-integrated pressure monitoring system designed to provide early warning alerts for the potential formation of pressure ulcers in various healthcare environments. The technology combines soft elastomer-encapsulated pressure sensors, wireless communication capabilities, and compact power management systems to continuously monitor and transmit real-time pressure data over extended periods, even in dynamic settings such as during surgery, patient transport, or daily activities at home. FEA results and extensive experimental evaluations demonstrate that the device maintains accurate and stable measurements when subjected to repeated loading, temperature fluctuations, and postural shifts. The integrated alert system provides timely vibratory and visual notifications, empowering patients and caregivers to take preventive measures whenever predefined thresholds are surpassed. Beyond hospital use, this platform offers a practical solution for outpatient settings and home care, potentially reducing the incidence of pressure ulcers, enhancing patient comfort, and lowering healthcare costs. Notably, the continuous data collected by our device could enable in-depth clinical studies to predict the onset, stage, and progression of pressure ulcers. Standardized protocols or widely accepted quantitative benchmarks for pressure ulcer generation do not yet exist. As such, the ability of this system to collect and analyze diverse factors, such as pressure level, cumulative load, and time duration, may offer value for clinical research in defining thresholds. These parameters are closely related to established ulcer-risk indicators, such as those reflected in the Braden or Norton scales. While direct correlation with clinical outcomes lies outside of the scope of this pilot study, future work will validate pressure profiles against clinical outcomes to inform predictive thresholds. By correlating these parameters with patient outcomes—such as the onset, progression, or worsening of pressure ulcers—researchers and clinicians may gain new insights into the mechanisms of pressure ulcer formation and individualized risk factors, thereby informing clinical guidelines and enabling personalized prevention strategies. For these reasons, and because the designs presented here rely on commercial components and manufacturing schemes that are compatible with volume production, these systems have the potential to modernize patient care protocols for managing pressure ulcers, as their long-lasting battery, wireless charging capability, biocompatible materials, and breathable design also enable multi-day monitoring. Data collected in this manner will not only provide additional insights into ulcer development and prevention but will also help address concerns about long-term wearability and clinical applicability.

## Methods

### Fabrication of a soft, elastomer-encapsulated pressure sensor

The process began with annealing the pressure sensor at 310 °C on a hot plate to dissolve the sealing adhesive between the sensor chip and the metal cap. This process enabled manual detachment of the metal cap using tweezers (Fig. S2A). After assembling the exposed sensor onto a FPCB, an elastomer structure was formed above the sensor using a three-dimensional-printed mold (Form 3B printer, Formlabs) that provides the design flexibility needed to optimize the structural parameters that affect pressure-sensing performance (Fig. S2B).

### Fabrication of the electronics

The FPCB design layouts were created using EAGLE CAD (Autodesk). After fabricating a soft, elastomer-encapsulated pressure sensor, all other components were mounted on a FPCB using surface-mounted technology.

### Encapsulation of the electronics in a soft enclosure

The electronics were encapsulated in a soft enclosure made from elastomers, designed using SOLIDWORKS 2022 software, using aluminum molds created through a milling machine (MDX-540, Rolland DGA), chosen for

their dimensional precision and durability, as critical for reproducible fabrication of the full elastomeric enclosure. Polyorganosiloxane (Silbione RTV 4420) cast into these molds formed the top encapsulating structures following thermal cure at 75 °C for 40 min. The bottom encapsulation layers were produced by spin-coating at 200 rpm on an acrylic plate, and then curing at 75 °C for 40 min. A fully populated FPCB was then aligned with the bottom layer, followed by casting uncured polyorganosiloxane elastomer (Ecoflex 00-30, Smooth-on), allowing it to cure at room temperature for 24 h after bringing the top and bottom layers together. This curing process securely bonds the top and bottom layers by filling the gap between them. This curing-induced integration provides robust encapsulation and long-term mechanical stability of the device under repeated loading/unloading cycles and during clinical use. Finally, laser cutting (CO<sub>2</sub> laser cutter, ULS) outlined the device and completed the fabrication process.

### Calibration of the pressure sensor

The response of a soft pressure sensor was calibrated as a function of the force applied using a motorized force tester (ESM303, Mark-10) with a 100 N force gauge (G1013, Mark-10). The applied pressure was then calculated based on the measured force and the surface area of the sensor by the sensor's surface area and the applied force.

### Finite element analysis

FEA was performed using ABAQUS (version 2022). The analysis used an implicit dynamic approach with a ramped load profile and a static step to remove residual effects. Contact interactions were defined for cushion–mattress, device–mattress, and skin–mattress interfaces with “hard” and frictionless behavior. Bones and circuit boards were embedded in soft tissue and elastomers, respectively. The model was subjected to body weight, with the mattress pinned at the bottom. For the heel model, a wrapping phase fixed the upper surface and applied pressure, which was later deactivated for loading. Contact between the cushion and body used “hard” and “rough” behavior. Different elements were used for components, and mesh convergence was verified. The Yeoh hyperelastic model captured the mechanical properties of Ecoflex, Silbione, and tissue. Details are in Note S1 and the parameters are in Table S3<sup>1,33–41</sup>.

### Human subject studies

Human subject studies involving the pressure monitoring device were conducted under approval from the Washington University in St. Louis Institutional Review Board (202104087) and healthy adult subjects under approval by the Northwestern University Institutional Review Board (STU00220120). The subjects participated following informed consent.

A padded dressing (e.g., Allevyn Gentle Border) containing the pressure monitoring device was applied to the sacrum and secured with a transparent film dressing (Tegaderm, 3M). A digital photograph was taken after application with the study ID label, excluding identifiable features. A triaxial accelerometer was placed on the operating bed or a non-sterile area of the patient using Tegaderm to record positional changes. The sensor remained in place throughout the surgery, continuously recording interface pressure. After the operation, both the dressing and accelerometer were removed. The skin was reassessed, documented in the CRF, and rephotographed. Foam dressings and film were discarded after each use. The pressure monitoring device was visually inspected and disinfected with a hospital-grade solution; damaged sensors were excluded from reuse and stored. More details are described in the IRB-approved study protocol.

All identifiable images in this study (Figs. 4, S5, and S6) were obtained and published with written informed consent from the participant. The participant explicitly consented to the publication of these photographs for scientific use.

### Data availability

The data that support the findings of this study are available within the main text and the Supplementary Information. All data are also available from the corresponding authors upon request.

Received: 11 August 2025; Accepted: 16 November 2025;

Published online: 03 December 2025

## References

- Schwartz, D. & Gefen, A. An integrated experimental-computational study of the microclimate under dressings applied to intact weight-bearing skin. *Int. Wound J.* **17**, 562–577 (2020).
- Gefen, A. How much time does it take to get a pressure ulcer? Integrated evidence from human, animal, and in vitro studies. *Ostomy Wound Manag.* **54**, 30–35 (2008).
- Asiri, S. Turning and repositioning frequency to prevent hospital-acquired pressure injuries among adult patients: systematic review. *Inquiry* **60**, 1–10 (2023).
- Ippolito, M. et al. The prevention of pressure injuries in the positioning and mobilization of patients in the ICU: a good clinical practice document by the Italian Society of Anesthesia, Analgesia, Resuscitation and Intensive Care. *J. Anesth. Analg. Crit. Care* **2**, 7 (2022).
- Palfreyman, S. J. & Stone, P. W. A systematic review of economic evaluations assessing interventions aimed at preventing or treating pressure ulcers. *Int. J. Nurs. Stud.* **52**, 769–788 (2015).
- Floyd, N. A. et al. The effectiveness of care bundles including the Braden Scale for preventing hospital-acquired pressure ulcers in older adults hospitalized in ICUs: a systematic review. *Open Nurs. J.* **15**, 74–84 (2021).
- Alderden, J. et al. Comparing risk profiles in critical care patients with Stage 2 and deep tissue pressure injuries. *JMIR Dermatol.* <https://doi.org/10.2196/29757> (2021).
- Evans, L. et al. Surviving sepsis campaign: international guidelines for management of sepsis and septic shock 2021. *Crit. Care Med.* **49**, e1066–e1111 (2021).
- Yoshikawa, T. T., Livesley, N. J. & Chow, A. W. Infected pressure ulcers in elderly individuals. *Clin. Infect. Dis.* **35**, 1390–1396 (2002).
- Mamom, J. et al. Electronic alert signal for early detection of tissue injuries in patients: an innovative pressure sensor mattress. *Diagnostics* **13**, 145 (2023).
- Hussain, A. M. Large area flexible piezoresistive sensor array for smart mattress application. *IEEE Sens. Lett.* **8**, 6006904 (2024).
- Han, S. et al. Battery-free, wireless sensors for full-body pressure and temperature mapping. *Sci. Transl. Med.* **10**, eaan4950 (2018).
- Oh, Y. S. et al. Battery-free, wireless soft sensors for continuous multi-site measurements of pressure and temperature from patients at risk for pressure injuries. *Nat. Commun.* **12**, 5008 (2021).
- Cho, S. et al. Wireless, multimodal sensors for continuous measurement of pressure, temperature, and hydration of patients in wheelchair. *npj Flex. Electron.* **7**, 8 (2023).
- Han, H. et al. Battery-free, wireless multi-modal sensor, and actuator array system for pressure injury prevention. *Small* **20**, e2405493 (2024).
- Choi, M. et al. Battery-free, wireless multi-sensing platform for comprehensive management of pressure injury and hygiene. *Adv. Funct. Mater.* **35**, e06774 (2025).
- Panula, T. et al. An instrument for measuring blood pressure and assessing cardiovascular health from the fingertip. *Biosens. Bioelectron.* **167**, 112483 (2020).
- Seo, S. G. et al. Minimally invasive, bioadaptive multimodal sensor probe with safe deployment for real-time acute compartment syndrome diagnosis. *Adv. Sci.* **12**, 2206942 (2025).
- Ha, K.-H. et al. Highly sensitive capacitive pressure sensors over a wide pressure range enabled by the hybrid responses of a highly porous nanocomposite. *Adv. Mater.* **33**, e2103320 (2021).
- Ha, K.-H. et al. Soft capacitive pressure sensors: trends, challenges, and perspectives. *ACS Nano* **16**, 3442–3448 (2022).
- Park, Y. et al. Soft, full Wheatstone bridge 3D pressure sensors for cardiovascular monitoring. *npj Flex. Electron.* **8**, 6 (2024).
- Grothier, L. Gentle foam dressings: interim results of an evaluation of the Allevyn range. *Br. J. Nurs.* **18**, S4–S10 (2024).
- Rose, A. Preventative dressings reduce postoperative tracheostomy-related pressure injury. *AACN Adv. Crit. Care* **34**, 148–153 (2023).
- Gibson, L. J. & Ashby, M. F. *Cellular Solids: Structure and Properties* 2nd edn (Cambridge University Press, 1997).
- Ramsteiner, F., Fell, N. & Forster, S. Testing the deformation behaviour of polymer foams. *Polym. Test.* **20**, 661–670 (2001).
- Choi, J. B. & Lakes, R. S. Analysis of elastic modulus of conventional foams and of re-entrant foam materials with a negative Poisson's ratio. *Int. J. Mech. Sci.* **37**, 51–59 (1995).
- Sun, Y. et al. The variation in elastic modulus throughout the compression of foam materials. *Acta Mater.* **110**, 161–174 (2016).
- Lobos, J. & Velankar, S. How much do nanoparticle fillers improve the modulus and strength of polymer foams? *J. Cell. Plast.* **52**, 57–88 (2016).
- Hasan, S. M., Touchet, T., Jayadeep, A. & Maitland, D. J. Controlling morphology and physio-chemical properties of stimulus-responsive polyurethane foams by altering chemical blowing agent content. *Polymers* **14**, 2288 (2022).
- Duygens, J., Clarac, F. & Cruse, H. Load-regulating mechanisms in gait and posture: comparative aspects. *Physiol. Rev.* **80**, 83–133 (2000).
- Hoque, E., Dickerson, R. F. & Stankovic, J. A. Monitoring body positions and movements during sleep using WISPs. In *Proc. Wireless Health*, San Diego, California, USA 44–53 (Association for Computing Machinery, 2010).
- Du, Y. et al. A skin-interfaced wireless wearable device and data analytics approach for sleep-stage and disorder detection. *Proc. Natl. Acad. Sci. USA* **122**, e2501220122 (2025).
- Kwak, S. S. et al. Skin-integrated devices with soft, holey architectures for wireless physiological monitoring, with applications in the neonatal intensive care unit. *Adv. Mater.* **33**, 2103974 (2021).
- Jeong, H. et al. Differential cardiopulmonary monitoring system for artifact-canceled physiological tracking of athletes, workers, and COVID-19 patients. *Sci. Adv.* **7**, eabg3092 (2021).
- Tsai, M.-Y., Chang, H.-Y. & Pecht, M. Warpage analysis of flip-chip PBGA packages subject to thermal loading. *IEEE Trans. Device Mater. Reliab.* **9**, 419–424 (2009).
- Zhang, C. et al. A representative-sandwich model for simultaneously coupled mechanical-electrical-thermal simulation of a lithium-ion cell under quasi-static indentation tests. *J. Power Sources* **298**, 309–321 (2015).
- Hong, T. T.-H. et al. The influence of mattress stiffness on spinal curvature and intervertebral disc stress—an experimental and computational study. *Biology* **11**, 1030 (2022).
- Sieracki, J. et al. Finite element analysis modeling of a novel silicone dressing. *Cureus* **12**, e10629 (2020).
- Kim, Y. K. Viscoelastic effect of FR-4 material on packaging stress development. *IEEE Trans. Adv. Packag.* **30**, 411–420 (2007).
- Hsu, J. T. & Vu-Quoc, L. A rational formulation of thermal circuit models for electrothermal simulation. I. Finite element method [power electronic systems]. *IEEE Trans. Circuits Syst. I Fund. Theory Appl.* **43**, 721–732 (1996).
- Sherwood, J. A. & Frost, C. C. Constitutive modeling and simulation of energy absorbing polyurethane foam under impact loading. *Polym. Eng. Sci.* **32**, 1138–1146 (1992).

## Acknowledgements

This work was supported by the Querrey Simpson Institute for Bioelectronics at Northwestern University. S.Y. acknowledges support from the National Research Foundation of Korea (NRF) grant (No. RS-2025-23525124), funded by the Korea government (MSIT), and the BK21 FOUR program (Digital Anti-aging Convergence Research Group, Inje University). Z.L. acknowledges support from the National Natural Science Foundation of China (12202241). K.K. acknowledges support from the National Research

Foundation of Korea (NRF) grant (Nos. RS-2022-NR072054 and RS-2020-NR049568) and the Institute of Information & Communications Technology Planning & Evaluation (IITP) under the Graduate School of Artificial Intelligence Semiconductor (IITP-2025-RS-2023-00256472) grant, funded by the Korea government (MSIT), and the BK21 FOUR program (Connected AI Education & Research Program for Industry and Society Innovation, KAIST EE, No. 4120200113769).

## Author contributions

S.Y., Z.L., N.F., J.-Y.Y., S.O., and K.-H.H. contributed equally to this work. S.Y., Y.H., J.S., and J.A.R. conceived and designed the research. S.Y., N.F., J.-Y.Y., S.O., K.-H.H., W.M.M., J.C., H.W., J.P., S.S.K., K.K., Y.P., D.C., H.-Y.A., C.P., S.K., T.W.P., W.-y.M., H.C.K., A.M.W., M.M., Y.H., J.S., and J.A.R. investigated and performed the experiments. S.Y., N.F., J.-Y.Y., S.O., and K.-H.H. conducted the data analysis. S.Y., Z.L., Y.H., and J.A.R. designed and conducted simulations. S.Y., Z.L., N.F., J.-Y.Y., S.O., K.-H.H., Y.P., J.S., and J.A.R. wrote the paper.

## Competing interests

J.A.R. serves on the editorial board, and Y.H. is an Associate Editor of *npj Flexible Electronics*. The authors declare no other competing interests.

## Additional information

**Supplementary information** The online version contains supplementary material available at

<https://doi.org/10.1038/s41528-025-00501-9>.

**Correspondence** and requests for materials should be addressed to Yonggang Huang, Justin Saks or John A. Rogers.

**Reprints and permissions information** is available at <http://www.nature.com/reprints>

**Publisher's note** Springer Nature remains neutral with regard to jurisdictional claims in published maps and institutional affiliations.

**Open Access** This article is licensed under a Creative Commons Attribution-NonCommercial-NoDerivatives 4.0 International License, which permits any non-commercial use, sharing, distribution and reproduction in any medium or format, as long as you give appropriate credit to the original author(s) and the source, provide a link to the Creative Commons licence, and indicate if you modified the licensed material. You do not have permission under this licence to share adapted material derived from this article or parts of it. The images or other third party material in this article are included in the article's Creative Commons licence, unless indicated otherwise in a credit line to the material. If material is not included in the article's Creative Commons licence and your intended use is not permitted by statutory regulation or exceeds the permitted use, you will need to obtain permission directly from the copyright holder. To view a copy of this licence, visit <http://creativecommons.org/licenses/by-nc-nd/4.0/>.

© The Author(s) 2025

<sup>1</sup>Querrey Simpson Institute for Bioelectronics, Northwestern University, Evanston, IL, USA. <sup>2</sup>School of Glocal Leaders, Glocal Honors College, Inje University, Gimhae, Republic of Korea. <sup>3</sup>College of Biomedical Science & Health, Inje University, Gimhae, Republic of Korea. <sup>4</sup>Department of Digital Anti-aging Healthcare, Graduate School of Inje University, Gimhae, Republic of Korea. <sup>5</sup>Department of Mechanical Engineering, Northwestern University, Evanston, IL, USA. <sup>6</sup>Division of Plastic and Reconstructive Surgery, Department of Surgery, Washington University in St. Louis, St. Louis, MO, USA. <sup>7</sup>Department of Semiconductor Convergence Engineering, Sungkyunkwan University, Suwon, Republic of Korea. <sup>8</sup>Division of Electrical Engineering, Hanyang University ERICA, Ansan, Republic of Korea. <sup>9</sup>School of Materials Science and Engineering, Gwangju Institute of Science and Technology, Gwangju, Republic of Korea. <sup>10</sup>Bionics Research Center of Biomedical Research Division, Korea Institute of Science and Technology, Seoul, Republic of Korea. <sup>11</sup>School of Electrical Engineering, Korea Advanced Institute of Science and Technology, Daejeon, Republic of Korea. <sup>12</sup>Department of Advanced Materials Engineering for Information and Electronics, Kyung Hee University, Yongin, Republic of Korea. <sup>13</sup>Thin Film Materials Research Center, Korea Research Institute of Chemical Technology, Daejeon, Republic of Korea. <sup>14</sup>Advanced Materials and Chemical Engineering, University of Science and Technology, Daejeon, Republic of Korea. <sup>15</sup>Department of Mechanical Engineering, University of Texas at Austin, Austin, TX, USA. <sup>16</sup>Department of Civil and Environmental Engineering, Northwestern University, Evanston, IL, USA. <sup>17</sup>Department of Materials Science and Engineering, Northwestern University, Evanston, IL, USA. <sup>18</sup>Department of Biomedical Engineering, Northwestern University, Evanston, IL, USA. <sup>19</sup>Department of Neurological Surgery, Feinberg School of Medicine, Northwestern University, Chicago, IL, USA. <sup>20</sup>These authors contributed equally: Seonggwang Yoo, Zengyao Lv, Nicholas Fadell, Jae-Young Yoo, Seyong Oh, Kyoung-Ho Ha. ✉e-mail: y-huang@northwestern.edu; jmsacks@wustl.edu; jrogers@northwestern.edu